JUSTC

Article

http://justc.ustc.edu.cn

Received: November 28, 2022; Accepted: March 02, 2023

Structure of the human CLC-7/Ostm1 complex reveals a novel state

Zhixuan Zhang*, Long Chen*, Jin He, and Ji She ✉

School of Life Sciences, Division of Life Sciences and Medicine, University of Science and Technology of China, Hefei 230027, China

* These authors contributed equally to this work

✉Correspondence: Ji She, E-mail: jishe@ustc.edu.cn

Graphical abstract

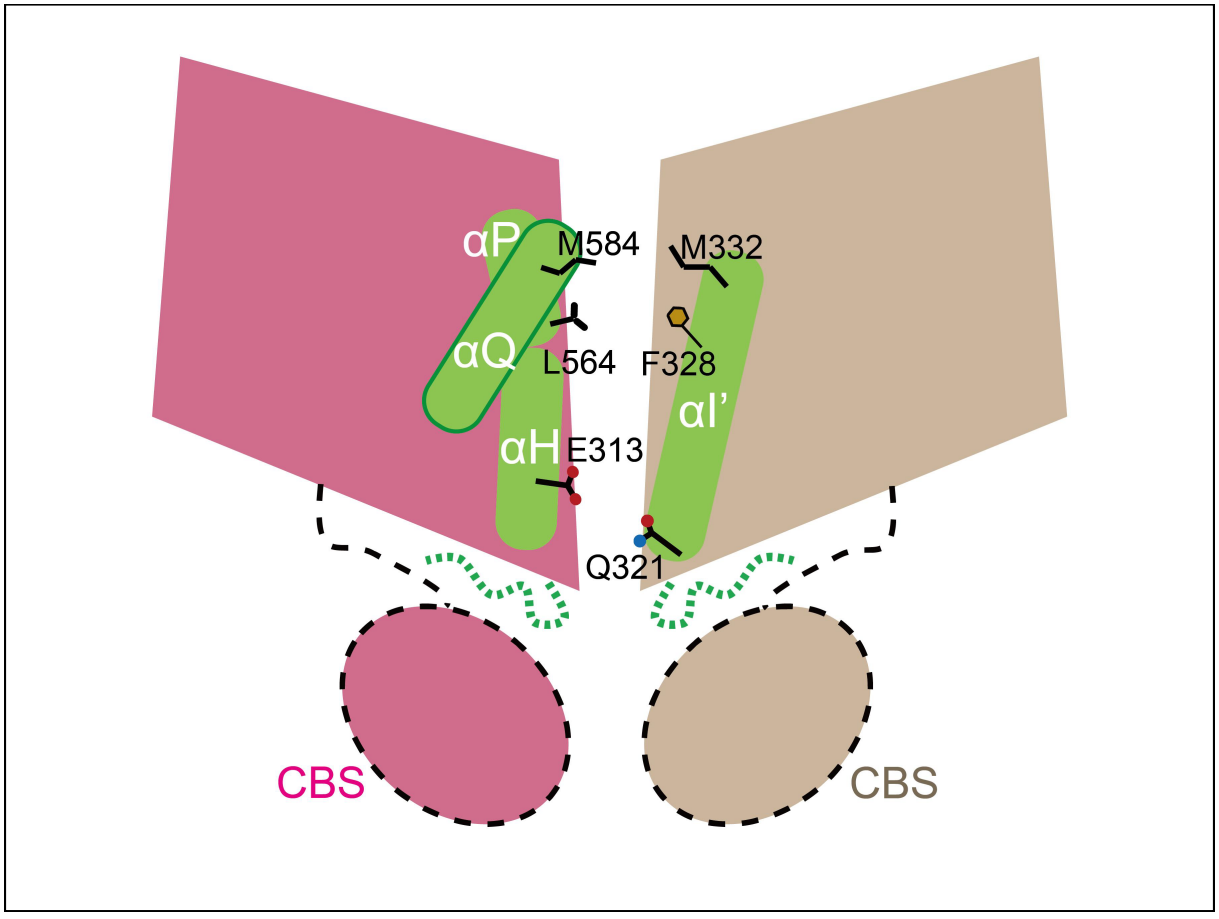

A novel conformational state of CLC-7.

Public summary

■ Structure of the human CLC-7/Ostm1 complex reveals a novel state with a disordered cytoplasmic domain.

■ The interface between the CLC-7 transmembrane domains is substantially reduced in the structure.

■ Key interactions involving multiple osteopetrosis-related residues are affected by the interface change.

Citation: Zhang Z X, Chen L, He J, et al. Structure of the human CLC-7/Ostm1 complex reveals a novel state. *JUSTC*, **2023**, 53(3): 0306. DOI: 10.52396/JUSTC-2022-0172

JUSTC

Article

http://justc.ustc.edu.cn

Received: November 28, 2022; Accepted: March 02, 2023

Structure of the human CLC-7/Ostm1 complex reveals a novel state

Zhixuan Zhang*, Long Chen*, Jin He, and Ji She ✉

School of Life Sciences, Division of Life Sciences and Medicine, University of Science and Technology of China, Hefei 230027, China

* These authors contributed equally to this work

✉Correspondence: Ji She, E-mail: jishe@ustc.edu.cn

Cite This: *JUSTC*, **2023**, 53(3): 0306 (6pp)

Read Online

SI Supporting Information

Abstract: CLC-7 functions as a Cl^-/H^+ exchanger in lysosomes. Defects in CLC-7 and its β-subunit, Ostm1, result in osteopetrosis and neurodegeneration. Here, we present the cryogenic electron microscopy (cryo-EM) structure of the human CLC-7/Ostm1 complex (HsCLC-7/Ostm1) at a resolution of 3.6 Å. Our structure reveals a new state of the CLC-7/Ostm1 heterotetramer, in which the cytoplasmic domain of CLC-7 is absent, likely due to high flexibility. The disordered cytoplasmic domain is probably not able to restrain CLC-7 subunits and thus allow their relative movements. The movements result in an approximately half smaller interface between the CLC-7 transmembrane domains than that in a previously reported CLC-7/Ostm1 structure with a well-folded cytoplasmic domain. Key interactions involving multiple osteopetrosis-related residues are affected by the interface change.

Keywords: CLC-7; Ostm1; osteopetrosis; chloride transporter; single-particle cryo-EM

CLC number: Q71 **Document code:** A

1 Introduction

CLC proteins are a family of transmembrane proteins mediating chloride ion (Cl^-) transport in all kingdoms of life[1–3]. In mammals, the CLC family contains both chloride channels and transporters. While CLC-1, CLC-2, and CLC-Ka/-Kb work as Cl^- channels on plasma membranes[4–6], CLC-3 to CLC-7 function as proton-coupled chloride transporters on endolysosomes[7–10], where they regulate the vesicular ion composition and facilitate their acidification by exchanging two Cl^- ions and one proton in the opposite direction. CLC-7 is a CLC transporter expressed on late endosomes/lysosomes and the ruffled border of osteoclasts[11]. It plays a key role in regulating lysosomal ion homeostasis and bone resorption[11,12]. CLC-7 deficiency causes osteopetrosis[11,13,14], a disease characterized by dense and fragile bone. More than ninety CLC-7 mutations have been identified to elicit osteopetrosis in humans[15]. CLC-7 mutations also result in neurodegeneration in the brain and retina due to impaired lysosomal digestion in neurons[12,16,17]. The function of CLC-7 requires a β-subunit, Ostm1, which is a single-pass transmembrane protein with a heavily glycosylated N-terminal domain (NTD) and a short cytosolic C-terminal region[17]. Ostm1 stabilizes CLC-7 in acidic lysosomes and is essential for the function of CLC-7[7,17]. Similar to CLC-7, Ostm1 mutations also result in severe osteopetrosis with neurodegeneration[13,18,19].

Structural and functional studies have provided important insights into the ion transport mechanisms of CLC family proteins[20–27]. CLCs form a dimeric structure with each subunit containing an ion conduction pathway. A glutamate in the pathway, named E_{gate}, is a critical gating residue for the ion conduction of CLC transporters[20,24]. Deprotonated E_{gate} can compete with Cl^- ions at two Cl^- binding sites and promote their release, whereas protonated E_{gate} allows the transfer of one proton in the opposite direction, leading to a $2Cl^-$: $1H^+$ exchange stoichiometry[23–25]. The ion transport pathway is divided into a proton pathway and a chloride pathway on the cytoplasmic side[25,28]. In the proton pathway, another glutamate, called E_{in}, mediates the transfer of a proton from or to E_{gate}. The direction of CLC ion conduction depends on the electrochemical gradient of Cl^- and H^+ ions. The structures of human CLC-7/Ostm1 and chicken CLC-7 with a stable cytoplasmic domain have been determined recently[26,27]. These studies defined the heterotetrametric architecture of CLC-7/Ostm1 proteins and provided important insights into the gating mechanism of CLC-7. Here, we present the structural analysis of the CLC-7/Ostm1 complex with a flexible cytoplasmic domain, revealing cytoplasmic domain-mediated regulation of the CLC-7 dimer.

2 Materials and methods

2.1 Protein expression and purification

Human CLC-7 (HsCLC-7, NCBI accession: NM_001287.6) and human Ostm1 (HsOstm1, NCBI accession: NM_014028.4) were cloned into a pEZT-BM vector[29] with a C-terminal 6x His tag and a C-terminal strep tag, respectively. Baculoviruses were generated in Sf9 cells (Thermo Fisher Scientific) following the standard protocol of the BacMam system (Thermo Fisher Scientific). The HsCLC-7/Ostm1 complex was heterologously expressed in HEK293F cells by infecting the cells with viruses at a ratio of 1 : 1 : 80

DOI: 10.52396/JUSTC-2022-0172

JUSTC, **2023**, 53(3): 0306

(HsCLC-7 virus : HsOstm1 virus : cells, v : v : v). Sodium butyrate (10 mmol/L) was added to the medium to boost protein expression. The purification protocol of the HsCLC-7/Ostm1 complex was similar to a previously reported protocol[30]. In brief, cells were homogenized by sonication on ice, and membrane proteins were extracted in a buffer containing 20 mmol/L Tris, pH 8.0, 150 mmol/L NaCl, 1% (w : v) n-dodecyl-β-D-maltopyranoside (DDM) (Anatrace) and 0.2% (w : v) cholesteryl hemisuccinate (CHS, Sigma Aldrich). After extraction and centrifugation, the supernatant was incubated with Strep-Tactin Sepharose (IBA Lifesciences) for 2 h with gentle agitation. The resin was then loaded on a disposable gravity column and washed with 10 column volumes of buffer A (20 mmol/L Tris, pH 8.0, 150 mmol/L NaCl and 0.06% glycol-diosgenin (GDN, Anatrace)). The HsCLC-7/Ostm1 complex was eluted with buffer A containing 2.5 mmol/L desthiobiotin and further purified by size exclusion chromatography on a Superose 6 column (GE Healthcare) preequilibrated with buffer A. The peak fraction was pooled and concentrated to 4.2 mg/mL for cryo-EM analysis.

2.2 EM data acquisition and image processing

The cryo-EM grids were prepared by plunge freezing using a Mark IV Vitrobot (FEI). Three microliters of HsCLC-7/Ostm1 (4.2 mg/mL) was applied to a glow-discharged Quantifoil R1.2/1.3 300-mesh gold holey carbon grid (Quantifoil, Micro Tools GmbH, Germany). Images were recorded with SerialEM on a Titan Krios microscope (FEI) operated at 300 kV with a K3 Summit direct electron detector (Gatan) in superresolution counting mode with a superresolution pixel size of 0.415 Å. The defocus range was set from –1.2 μm to –2.8 μm. Each micrograph was dose-fractionated to 32 frames with a total exposure time of 1.6 s, resulting in a total dose of approximately 64 $e^{-}/Å^{2}$.

Micrographs were motion corrected and binned 2-fold (yielding a pixel size of 0.83 Å/pixel) with MotionCor2[31]. The CTF parameters of the micrographs were estimated using the GCTF program[32]. All other steps of image processing were performed using RELION 3.0[33]. A small set of particles was manually picked and used to generate class averages by 2D classification for automatic particle picking. A total of 3,063,318 particles were picked from the full dataset of 5,948 micrographs. The particles were extracted and binned 4 times (3.32 Å/pixel). After 2D classification, a total of 2,872,902 particles were selected for 3D classification. The HsCLC-1 structure (PDB accession number 6COY) was used as the initial reference map. After two rounds of 3D classifications, the 3D classes showing good secondary structure features were selected and re-extracted into the original pixel size of 0.83 Å. One round of 3D refinement with C2 symmetry imposed resulted in a 3D reconstruction with a resolution of 4.2 Å (~704,000 particles). Another round of 3D classification with local angular search was then performed, and two good classes (~199,000 particles) were selected for CTF refinement and 3D refinement, which resulted in a map at a resolution of 3.6 Å.

All resolutions were estimated by applying a soft mask around the protein density and the gold-standard Fourier shell correlation (FSC) = 0.143 criterion. ResMap was used to calculate the local resolution map[34].

2.3 Model building, refinement, and validation

Model buildings were conducted in Coot[35]. The human CLC-1 structure (PDB accession number 6COY) was used as the reference for the model building of CLC-7. The luminal domain of Ostm1 was automatically built by Phenix[36] and then manually adjusted in Coot. Real-space model refinement[37] and validation[38] were performed in Phenix. The final model contains residues 118–265 and 277–608 for CLC-7 and residues 76–131, 143–203, and 221–306 for Ostm1. The statistics of the model geometries were generated using MolProbity[39]. All figures were prepared using PyMol (RRID: SCR_000305, The PyMOL Molecular Graphics System, Version 1.8 Schrödinger, LLC.), Chimera[40] or ChimeraX[41]. We used the PDBePISA tool to calculate protein – protein interfaces[42].

2.4 Data availability

The cryo-EM map of the CLC-7/Ostm1 complex in this study and its associated atomic model have been deposited in the wwPDB OneDep System under EMD accession code EMD-35048 and PDB ID code 8HVT, respectively.

3 Results

3.1 Overall structure of the HsCLC-7/Ostm1 complex

The structure of the HsCLC-7/Ostm1 complex was determined to a resolution of 3.6 Å using single-particle cryo-EM (Fig. 1a–c, Table 1, and Figs. S1, S2). Similar to previous CLC-7/Ostm1 structures[26, 27], HsCLC-7 forms a dimer with each subunit interacting with one Ostm1, leading to the stoichiometry of CLC-7 to Ostm1 being one to one. Each CLC-7 contains an ion conduction pathway, which is similar to that of the *E. coli* CLC transporter (EcCLC)[24], indicating a conserved ion transport mechanism. The gating glutamate (Glu247) points toward the luminal side, adopting an "up" conformation (Fig. 1d). The N-terminal domain of Ostm1 forms a dimer in the lysosomal lumen, sitting atop dimeric CLC-7, while the transmembrane helix of Ostm1 tightly packs with the transmembrane domain of CLC-7 (Fig. 1a–c). The detailed interactions between Ostm1 and CLC-7 in the current structure will not be discussed, as they are essentially the same as those in previous CLC-7/Ostm1 structures[26, 27]. However, different from previously reported CLC-7/Ostm1 structures, the cytoplasmic domain of CLC-7 shows weak density in our current map (Fig. S1i), possibly due to its high flexibility. We will hereafter refer to the HsCLC-7/Ostm1 structure with or without a stable cytoplasmic domain as CLC-7-stable (7JM7) and CLC-7-flexible (the structure in the current study), respectively.

Previous studies have shown that the cytoplasmic domain of CLC-7 is formed by two cystathionine-β-synthase (CBS) domains, the N-terminus, and an ATP molecule[26]. The ATP molecule interacts with the two CBS domains and the N-terminus[26] and thus has a key role in stabilizing the cytoplasmic domain. As the full-length CLC-7 protein was expressed in the current study (Fig. S1a) and some weak density of the cytoplasmic domain can be observed in the 2D class averages (Fig. S1c), we suspect that one possible reason for the

DOI: 10.52396/JUSTC-2022-0172
JUSTC, **2023**, 53(3): 0306

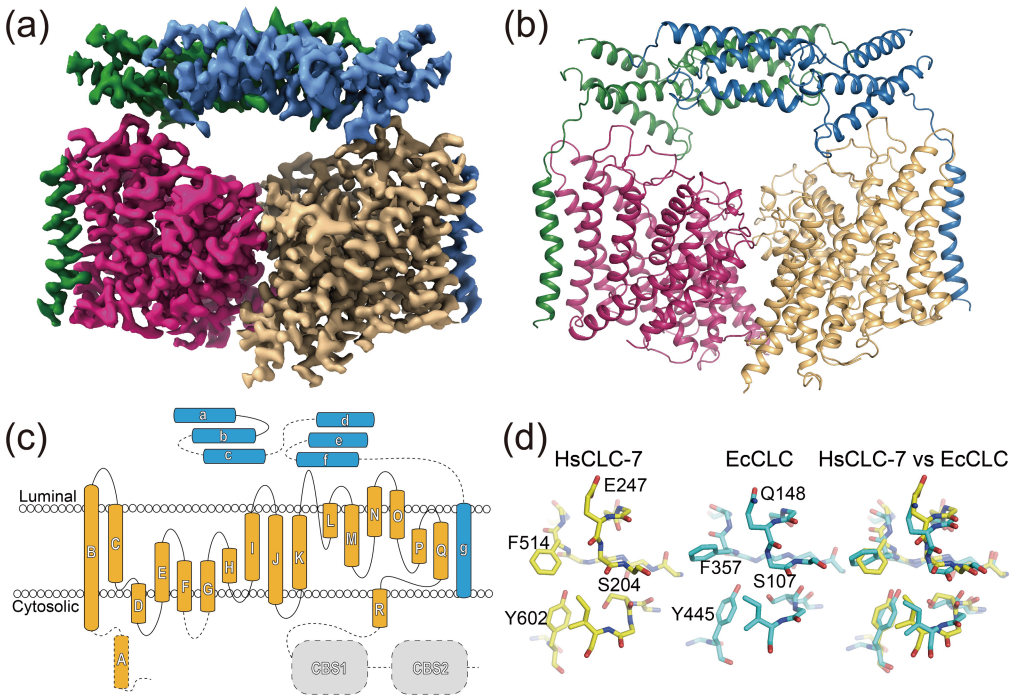

Fig. 1. Overall structure of the HsCLC-7/Ostm1 complex. (a, b) 3D reconstruction (a) and cartoon representation (b) of the HsCLC-7/Ostm1 complex with each subunit in individual colors. (c) Topology of one HsCLC-7 subunit (orange) and one Ostm1 subunit (cyan). Dashed lines indicate flexible regions absent in the structure. (d) Comparison of the ion conduction pathways of HsCLC-7 and EcCLC.

Table 1. Cryo-EM data acquisition, reconstruction and model refinement statistics.

	HsCLC-7/Ostm1
Data collection and processing	
Microscope/Detector	K3
Image software and collection	SerialEM
Voltage (kV)	300
Electron exposure (e$^-$/Å^2)	64
Defocus range (μm)	−1.2 to −2.8
Pixel size (Å)	0.83
Micrographs	5,948
Symmetry imposed	C2
Initial particle images	3,063,318
Final particle images	~199 K
Map resolution (Å)	3.6
FSC threshold	0.143
Refinement	
Initial model used	HsCLC-1(PDB: 6COY)
Model resolution (Å)	3.7
FSC threshold	0.5
Model composition	
Non-Hydrogen atoms	10,702
Protein residues	1,366
Ligands	BMA: 2 NAG: 10
B factors (Å^2)	
Protein	61.09
Ligand	85.05
R.m.s. deviations	
Bond lengths (Å)	0.009
Bond angles (°)	1.085
Validation	
MolProbity score	1.72
Clash score	5.55
Poor rotamers (%)	0.00
Ramachandran plot	
Favored (%)	93.61
Allowed (%)	6.39
Disallowed (%)	0.00

missing cytoplasmic domain is that the ATP molecule is washed out during purification, and the cytoplasmic domain cannot maintain a stable conformation in the absence of ATP.

3.2 Cytoplasmic domain regulates the dimer interface

To reveal the potential structural change induced by the cytoplasmic domain, we compared the structures with or without a stable cytoplasmic domain (Fig. 2a). Single subunits in the CLC-7-stable and CLC-7-flexible structures are virtually identical with a backbone RMSD of 0.5 Å, indicating reliable structure determination. However, the dimeric structures cannot be aligned well. When one subunit was aligned, a large shift of the transmembrane domain of the opposite subunit was observed (Fig. 2a). In the CLC-7-stable structure, the transmembrane dimer interface is primarily formed by hydrophobic residues with a large calculated interface of ~1,762 Å^2 (Fig. 2b). The relative movement of dimeric subunits in CLC-7-flexible efficiently reduces the interface to ~843 Å^2, and fewer residues contribute to dimer formation (Fig. 2b, c). In addition, several detergent-like or lipid-like molecules were observed to insert in the gap between the two subunits of the CLC-7-flexible structure from the cytosolic side (Fig. 2d, e). The state change of the cytoplasmic domains may play a critical role in regulating the dimer interface. A well-folded cytoplasmic domain holds and stabilizes the CLC-7 dimer by interacting with both the transmembrane domain and the neighboring cytoplasmic domain[26,27] (Fig. 2f). In contrast, the flexible cytoplasmic domain cannot restrain two subunits, allowing the relative movement.

3.3 Disease-related residues on the dimer interface

Several disease-related residues are located on the transmembrane dimer interface of CLC-7. Missense mutations of these

DOI: 10.52396/JUSTC-2022-0172
JUSTC, **2023**, 53(3): 0306

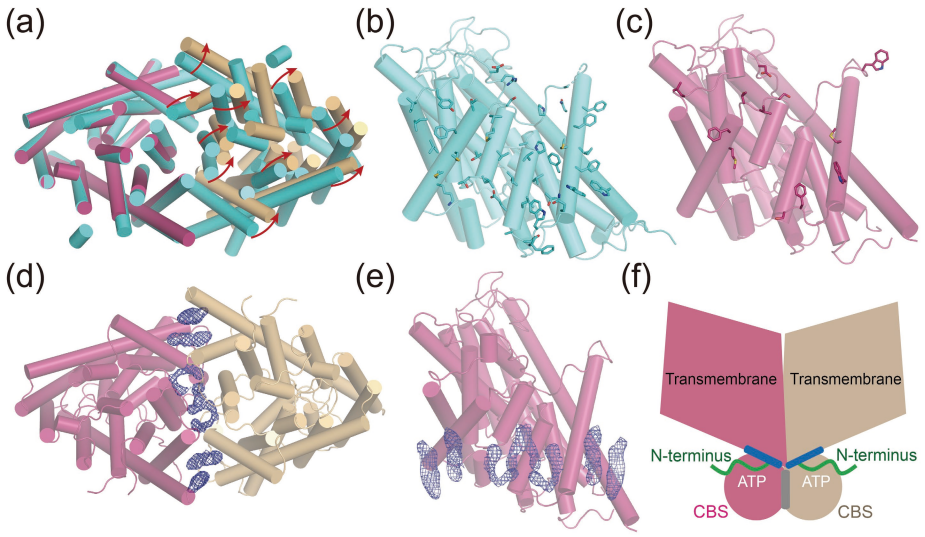

Fig. 2. Dimer interface of HsCLC-7. (a) Comparison of the transmembrane domains of the CLC-7 flexible (purple and orange) and CLC-7 stable (7JM7, cyan) structures (bottom view). Arrows indicate the shifts of helices. Linkers between helices are omitted for clarity. (b, c) Side view of the dimer interface of the CLC-7-stable (b) and CLC-7-flexible (c) structures. Residues on the interface are shown as sticks. (d, e) Bottom view (d) and side view (e) of the HsCLC-7-flexible structure with lipid density shown as blue mesh. (f) Cartoon representation of the CLC-stable structure. Ostm1 is not shown here. Blue bars indicate the interfaces between the cytoplasmic domain and the transmembrane domain, and the gray bar indicates the interface between the cytoplasmic domains. The cytoplasmic domain consists of CBS domains, the N-terminus, and an ATP molecule.

residues, including Leu564Pro, Met332Val, and Glu313Lys, cause autosomal recessive osteopetrosis or autosomal dominant osteopetrosis type II[43–45]. In the CLC-7-stable structure, Leu564 on helix αQ establishes hydrophobic interactions with Phe328 on helix αI' (the apostrophe indicates the helix from the neighboring subunit), while Met332 on helix αI' interacts with Met584 on helix αQ. However, in the CLC-7-flexible structure, helix αI' shifts away from the neighboring subunit by ~5.4 Å, resulting in the loss of the interactions mentioned above (Fig. 3a). Another important interaction at the dimer interface is formed by Glu313 on helix αH and Gln321 on helix αI' in the CLC-7-stable structure (Fig. 3b). Glu313 and Gln321 mutants were previously reported to exhibit accelerated voltage-dependent activation[27], and they were suggested to regulate slow gating of CLC-7 by affecting proton transport, as Glu313 is close to the proton glutamate (E_{in}, Glu314).

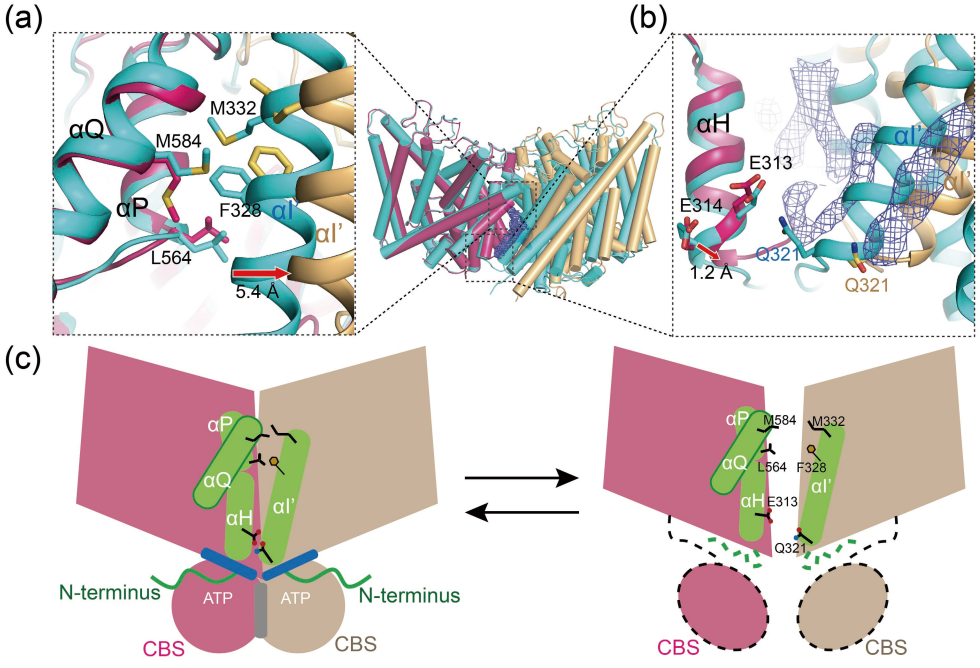

Fig. 3. Disease-related residues on the dimer interface of HsCLC-7. (a, b) Detailed interaction changes between CLC-7-flexible (purple and orange) and CLC-7-stable (cyan). Key residues are shown as sticks. Lipids in (a) are omitted for clarity. (c) Working model of HsCLC-7 regulation by the cytoplasmic domain-mediated dimer change. The left panel shows the CLC-7 state with a well-folded cytoplasmic domain consisting of CBS domains, the N-terminus, and ATP. The right panel shows the CLC-7 state with disordered N-terminus and CBS domains.

DOI: 10.52396/JUSTC-2022-0172
JUSTC, **2023**, 53(3): 0306

In the current structure, the interaction between Glu313 and Gln321 is also destroyed (Fig. 3b). Moreover, the Cα of the proton glutamate Glu314 shows a 1.2 Å shift from that in the CLC-7-stable structure, which may contribute to the kinetics change. As these disease-related residues probably have important functional or structural roles, the interface change caused by the cytoplasmic domain state switch is likely to be an important way to regulate the function of CLC-7.

4 Discussion

In the current study, we report a novel dimeric state of the HsCLC-7/Ostm1 complex (Fig. 3c). The lack of a stable cytoplasmic domain leads to a large relative shift between the dimeric subunits, which results in a much smaller dimer interface. Several interactions involving disease-related residues are affected by the dimer interface change. Because ATP has a central role in stabilizing the cytoplasmic domain of CLC-7[26], it is likely to be an important factor in regulating the state of the cytoplasmic domain and dimer interface formation. Indeed, several CLCs, including CLC-2, CLC-4, and AtCLCa, are known to be regulated by ATP binding[46–48]. Although ATP showed no obvious effect on the transport of CLC-7 in one study[7], multiple osteopetrosis-causing mutations of CLC-7 are located around the ATP binding site[26,44,49], indicating the significance of ATP binding.

Several structures of mammalian CLCs have been reported thus far. The structures of human CLC-1 with or without a stable cytoplasmic domain exhibited no major difference in the dimer interface of the transmembrane domain[22,50]. However, the comparison of two bovine CLC-K structures showed that its dimer interface can be affected by two inserted lipid molecules[21]. As the cytoplasmic domains have ordered structures in both CLC-K structures, the change in interface area is smaller than that of CLC-7. For other mammalian CLCs, only the structure of CLC-5 CBS domains in complex with ATP is known[51], and the full-length structures are still unavailable. It will be interesting to study whether these CLC transporters exhibit an interface change similar to that of CLC-7 presented in the current study. Together, this study reveals a new structural state of the CLC-7/Ostm1 complex and provides a foundation for further mechanistic studies of CLC transport and regulation.

Supporting information

The supporting information for this article can be found online at https://doi.org/10.52396/JUSTC-2022-0172. There are two figures in the supporting information.

Acknowledgements

This work was supported by the Ministry of Science and Technology of China (2021YFF0600801), the National Natural Science Foundation of China (32071201), and the Fundamental Research Funds for the Central Universities (WK2070000183).

Conflict of interest

The authors declare that they have no conflict of interest.

Biographies

Zhixuan Zhang is currently a master's student under the supervision of Prof. Ji She at the University of Science and Technology of China. His research mainly focuses on the structure and function of membrane transporters.

Long Chen is currently a Ph.D. student under the supervision of Prof. Ji She at the University of Science and Technology of China. His research mainly focuses on the structure and function of membrane transporters.

Ji She is currently a Professor at the Division of Life Sciences and Medicine, University of Science and Technology of China. He received his Ph.D. degree in Physiology from Perking University. His research interests include ion transport mechanisms, the structure and function of transporters, and structure-based drug studies.

References

[1] Jentsch T J. Discovery of CLC transport proteins: Cloning, structure, function and pathophysiology. *J. Physiol.* , **2015**, *593* (18): 4091–4109.
[2] Jentsch T J, Neagoe I, Scheel O. CLC chloride channels and transporters. *Curr. Opin. Neurobiol.* , **2005**, *15* (3): 319–325.
[3] Jentsch T J, Pusch M. CLC chloride channels and transporters: Structure, function, physiology, and disease. *Physiol. Rev.* , **2018**, *98* (3): 1493–1590.
[4] Steinmeyer K, Ortland C, Jentsch T J. Primary structure and functional expression of a developmentally regulated skeletal muscle chloride channel. *Nature,* **1991**, *354*: 301–304.
[5] Thiemann A, Gründer S, Pusch M, et al. A chloride channel widely expressed in epithelial and non-epithelial cells. *Nature,* **1992**, *356*: 57–60.
[6] Kieferle S, Fong P, Bens M, et al. Two highly homologous members of the ClC chloride channel family in both rat and human kidney. *Proc. Natl. Acad. Sci. U. S. A.* , **1994**, *91* (15): 6943–6947.
[7] Leisle L, Ludwig C F, Wagner F A, et al. ClC-7 is a slowly voltage-gated $2Cl^-/1H^+$-exchanger and requires Ostm1 for transport activity. *EMBO J.,* **2011**, *30* (11): 2140–2152.
[8] Scheel O, Zdebik A A, Lourdel S, et al. Voltage-dependent electrogenic chloride/proton exchange by endosomal CLC proteins. *Nature,* **2005**, *436*: 424–427.
[9] Neagoe I, Stauber T, Fidzinski P, et al. The late endosomal ClC-6 mediates proton/chloride countertransport in heterologous plasma membrane expression. *J. Biol. Chem.* , **2010**, *285* (28): 21689–21697.
[10] Picollo A, Pusch M. Chloride/proton antiporter activity of mammalian CLC proteins ClC-4 and ClC-5. *Nature,* **2005**, *436*: 420–423.
[11] Kornak U, Kasper D, Bösl M R, et al. Loss of the ClC-7 chloride channel leads to osteopetrosis in mice and man. *Cell,* **2001**, *104* (2): 205–215.
[12] Kasper D, Planells-Cases R, Fuhrmann J C, et al. Loss of the chloride channel ClC-7 leads to lysosomal storage disease and neurodegeneration. *EMBO J.,* **2005**, *24* (5): 1079–1091.
[13] Sobacchi C, Schulz A, Coxon F P, et al. Osteopetrosis: Genetics, treatment and new insights into osteoclast function. *Nat. Rev. Endocrinol.,* **2013**, *9* (9): 522–536.
[14] Weinert S, Jabs S, Supanchart C, et al. Lysosomal pathology and osteopetrosis upon loss of H^+-driven lysosomal Cl- accumulation. *Science,* **2010**, *328*: 1401–1403.
[15] Zifarelli G. The role of the lysosomal Cl^-/H^+antiporter ClC-7 in osteopetrosis and neurodegeneration. *Cells,* **2022**, *11* (3): 366.
[16] Pressey S N R, O'Donnell K J, Stauber T, et al. Distinct neuropathologic phenotypes after disrupting the chloride transport

DOI: 10.52396/JUSTC-2022-0172
JUSTC, **2023**, 53(3): 0306

proteins ClC-6 or ClC-7/Ostm1. *J. Neuropathol. Exp. Neurol.,* **2010**, *69* (12): 1228–1246.
[17] Lange P F, Wartosch L, Jentsch T J, et al. ClC-7 requires Ostm1 as a beta-subunit to support bone resorption and lysosomal function. *Nature,* **2006**, *440*: 220–223.
[18] Pangrazio A, Poliani P L, Megarbane A, et al. Mutations in OSTM1 (grey lethal) define a particularly severe form of autosomal recessive osteopetrosis with neural involvement. *J. Bone Miner. Res. ,* **2006**, *21* (7): 1098–1105.
[19] Castellano Chiodo D, DiRocco M, Gandolfo C, et al. Neuroimaging findings in malignant infantile osteopetrosis due to OSTM1 mutations. *Neuropediatrics,* **2007**, *38* (3): 154–156.
[20] Dutzler R, Campbell E B, Cadene M, et al. X-ray structure of a ClC chloride channel at 3.0 Å reveals the molecular basis of anion selectivity. *Nature,* **2002**, *415*: 287–294.
[21] Park E, Campbell E B, MacKinnon R. Structure of a CLC chloride ion channel by cryo-electron microscopy. *Nature,* **2017**, *541*: 500–505.
[22] Park E, MacKinnon R. Structure of the CLC-1 chloride channel from Homo sapiens. *eLife,* **2018**, *7*: e36629.
[23] Feng L, Campbell E B, Hsiung Y, et al. Structure of a eukaryotic CLC transporter defines an intermediate state in the transport cycle. *Science,* **2010**, *330*: 635–641.
[24] Dutzler R, Campbell E B, MacKinnon R. Gating the selectivity filter in ClC chloride channels. *Science,* **2003**, *300*: 108–112.
[25] Feng L, Campbell E B, MacKinnon R. Molecular mechanism of proton transport in CLC Cl^-/H^+ exchange transporters. *Proc. Natl. Acad. Sci. U. S. A.,* **2012**, *109* (29): 11699–11704.
[26] Schrecker M, Korobenko J, Hite R K. Cryo-EM structure of the lysosomal chloride-proton exchanger CLC-7 in complex with OSTM1. *eLife,* **2020**, *9*: e59555.
[27] Zhang S, Liu Y, Zhang B, et al. Molecular insights into the human CLC-7/Ostm1 transporter. *Sci. Adv.,* **2020**, *6* (33): eabb4747.
[28] Accardi A, Walden M, Nguitragool W, et al. Separate ion pathways in a Cl^-/H^+ exchanger. *J. Gen. Physiol.,* **2005**, *126* (6): 563–570.
[29] Morales-Perez C L, Noviello C M, Hibbs R E. Manipulation of subunit stoichiometry in heteromeric membrane proteins. *Structure,* **2016**, *24* (5): 797–805.
[30] She J, Zeng W, Guo J, et al. Structural mechanisms of phospholipid activation of the human TPC2 channel. *eLife,* **2019**, *8*: e45222.
[31] Zheng S Q, Palovcak E, Armache J P, et al. MotionCor2: Anisotropic correction of beam-induced motion for improved cryo-electron microscopy. *Nat. Methods,* **2017**, *14* (4): 331–332.
[32] Zhang K. Gctf: Real-time CTF determination and correction. *J. Struct. Biol.,* **2016**, *193* (1): 1–12.
[33] Kimanius D, Forsberg B O, Scheres S H, et al. Accelerated cryo-EM structure determination with parallelisation using GPUs in RELION-2. *eLife,* **2016**, *5*: e18722.
[34] Kucukelbir A, Sigworth F J, Tagare H D. Quantifying the local resolution of cryo-EM density maps. *Nat. Methods,* **2014**, *11* (1): 63–65.
[35] Emsley P, Lohkamp B, Scott W G, et al. Features and development of Coot. *Acta Crystallogr. D Biol. Crystallogr.,* **2010**, *66*: 486–501.
[36] Terwilliger T C, Adams P D, Afonine P V, et al. A fully automatic method yielding initial models from high-resolution cryo-electron microscopy maps. *Nat. Methods,* **2018**, *15* (11): 905–908.
[37] Afonine P V, Poon B K, Read R J, et al. Real-space refinement in PHENIX for cryo-EM and crystallography. *Acta Crystallogr. D Struct. Biol.,* **2018**, *74*: 531–544.
[38] Afonine P V, Klaholz B P, Moriarty N W, et al. New tools for the analysis and validation of cryo-EM maps and atomic models. *Acta Crystallogr. D Struct. Biol.,* **2018**, *74*: 814–840.
[39] Chen V B, Arendall III W B, Headd J J, et al. MolProbity: All-atom structure validation for macromolecular crystallography. *Acta Crystallographica Section D,* **2020**, *66*: 12–21.
[40] Pettersen E F, Goddard T D, Huang C C, et al. UCSF Chimera: A visualization system for exploratory research and analysis. *J. Comput. Chem.,* **2004**, *25* (13): 1605–1612.
[41] Goddard T D, Huang C C, Meng E C, et al. UCSF ChimeraX: Meeting modern challenges in visualization and analysis. *Protein Sci.,* **2018**, *27* (1): 14–25.
[42] Krissinel E, Henrick K. Inference of macromolecular assemblies from crystalline state. *J Mol Biol.,* **2007**, *372* (3): 774–797.
[43] Pang Q, Chi Y, Zhao Z, et al. Novel mutations of *CLCN7* cause autosomal dominant osteopetrosis type II (ADO-II) and intermediate autosomal recessive osteopetrosis (IARO) in Chinese patients. *Osteoporos. Int.,* **2016**, *27* (3): 1047–1055.
[44] Frattini A, Pangrazio A, Susani L, et al. Chloride channel *ClCN7* mutations are responsible for severe recessive, dominant, and intermediate osteopetrosis. *J. Bone Miner Res.,* **2003**, *18* (10): 1740–1747.
[45] Wang C, Zhang H, He J W, et al. The virulence gene and clinical phenotypes of osteopetrosis in the Chinese population: Six novel mutations of the *CLCN7* gene in twelve osteopetrosis families. *J. Bone Miner Metab.,* **2012**, *30* (3): 338–348.
[46] De Angeli A, Moran O, Wege S, et al. ATP binding to the C terminus of the *Arabidopsis thaliana* nitrate/proton antiporter, AtCLCa, regulates nitrate transport into plant vacuoles. *J. Biol. Chem.,* **2009**, *284* (39): 26526–26532.
[47] Stölting G, Teodorescu G, Begemann B, et al. Regulation of ClC-2 gating by intracellular ATP. *Pflugers Arch-Eur J Physiol,* **2013**, *465*: 1423–1437.
[48] Vanoye C G, George A L Jr. Functional characterization of recombinant human ClC-4 chloride channels in cultured mammalian cells. *J. Physiol.,* **2002**, *539*: 373–383.
[49] Cleiren E, Bénichou O, Van Hul E, et al. Albers-Schönberg disease (autosomal dominant osteopetrosis, type II) results from mutations in the *ClCN7* chloride channel gene. *Human Molecular Genetics,* **2001**, *10* (25): 2861–2867.
[50] Wang K, Preisler S S, Zhang L, et al. Structure of the human ClC-1 chloride channel. *PLoS Biol.,* **2019**, *17* (4): e3000218.
[51] Meyer S, Savaresi S, Forster I C, et al. Nucleotide recognition by the cytoplasmic domain of the human chloride transporter ClC-5. *Nat. Struct. Mol. Biol.,* **2007**, *14*: 60–67.

DOI: 10.52396/JUSTC-2022-0172
JUSTC, **2023**, 53(3): 0306